ators of the excitations, $\alpha_q^\dagger$ and α_q, respectively, by the following equations:

$$\gamma_q = -(u_q + v_q)\alpha_q^\dagger + \alpha_{-q}) , \tag{36}$$

$$\gamma_q|0\rangle = -(u_q + v_q)\alpha_q^\dagger|0\rangle . \tag{37}$$

Hence, $$(u_q + v_q)^2 = \langle 0|\gamma_q\gamma_{-q}|0\rangle . \tag{38}$$

For brevity we denote the ground-state expectation value of $\gamma_q\gamma_{-q}$ by F_q. The equations determining the u's and v's will be

$$(u_q + v_q)^2 = F_q , \tag{39}$$

$$u_q^2 - v_q^2 = 1 . \tag{40}$$

The solutions are

$$u_q^2 = (F_q + 1)^2/4F_q , \tag{41}$$

$$v_q^2 = (F_q - 1)^2/4F_q . \tag{42}$$

Hence, the u's and v's can be determined from the ground-state properties of the system.

VI. SUMMARY

A systematic approximation scheme based on the assumption of small density and current fluctuations was presented. The operators ρ_q and $\Gamma_p^\dagger$ appearing in the Hamiltonian were expanded, using the above assumption, in terms of simple operators. The possibility of obtaining the excitation wave functions and spectrum to any desired order, either by using known ground-state expectation values or by using the procedure described in Sec. IV, is outlined. Hence, this method allows one to obtain the interquasiparticle interactions. To demonstrate the applicability of the method, it was shown that the first-order calculation yields the well-known Feynman results as well as the results of Bogoliubov and Pitayevski. It was further shown that second-order calculations yield the improved result of Feynman and Cohen.

ACKNOWLEDGMENT

I wish to thank Professor M. Luban for reading the manuscript and making some helpful remarks.

[1]L. P. Pitayevski, Zh. Eksperim. i Teor. Fiz. 31, 536 (1956) [Soviet Phys. JETP 4, 439 (1957)].

[2]N. N. Bogoliubov, J. Phys. USSR 11, 23 (1947).

[3]R. P. Feynman, Phys. Rev. 94, 262 (1954).

[4]R. P. Feynman and M. Cohen, Phys. Rev. 102, 1189 (1956).

[5]D. Pines, in *Many-Body Theory*, edited by Ryogo-Kubo (Benjamin, New York, 1962), part 1.

[6]R. F. Dashen and D. H. Sharp, Phys. Rev. 165, 1857 (1968).

[7]D. H. Sharp, Phys. Rev. 165, 1867 (1968).

[8]D. J. Gross, Phys. Rev. 177, 1 (1969).

[9]The potential between two helium atoms, conventionally used, does not have a Fourier transform. Such a potential however has recently been applied to real He^4 by N. Mihara and R. D. Ruff, Phys. Rev. 174, 221 (1968). Anyhow, the results relating energy spectrum to measurable ground-state properties of the system are valid regardless of the form of the potential used.

[10]A. Thellung, Nuovo Cimento 9, 243 (1958), Suppl. 1.

PHYSICAL REVIEW A VOLUME 2, NUMBER 1 JULY 1970

Theory of Gas Lasers and Its Application to an Experiment

Helen K. Holt

National Bureau of Standards, Washington, D. C. 20234

(Received 26 March 1969; revised manuscript received 20 February 1970)

The semiclassical theory of gas lasers has been reformulated by adding rate terms to the density-matrix component differential equations. The solution to these equations, in the form of a Fourier series, is applicable at high laser intensities. A calculation of the effect of phase-changing collisions is also included so that the results can be compared to experimental data taken with a He-Ne laser operating at a wavelength of 1.15 μm.

I. INTRODUCTION

Lamb's semiclassical theory of the gas laser[1] accurately predicts many laser properties, such as the power output and the frequency as a function of cavity length. However, as Lamb points out, the applicability of his third-order results is limited to low laser powers. Bennett's hole-burning theory[2] is more heuristic and gives results equivalent to those of Ref. 1 at low intensities. At-

tempts to extend Lamb's theory to fifth order in the electric field[3] lead to cumbersome expressions which necessitate many approximations. In addition, the iterative approach of Refs. 1 and 3 seems to lead to an asymptotic series which cannot be used if the electric field is large. The results of Refs. 1 and 2 are also limited to atoms for which the width of the velocity distribution is large compared to the natural widths of the laser levels.

Recently there have been several papers on the theory of high-intensity lasers which use the semiclassical approach.[4–6] The results of Refs. 4 and 5 seem to be equivalent; they are useful at higher laser intensities than the theories of Refs. 1 and 2. Effects due to low-velocity atoms are neglected, however; these effects become important at high intensities and when the Doppler width of the laser transition is not large compared to the natural widths. The Stenholm-Lamb theory[6] is useful at higher intensities than the results of Refs. 4 and 5 and includes some interesting features not present in the other theories. The theoretical results of the present paper are equivalent to those of the Stenholm-Lamb paper, although the approach is different.

The purpose of the present paper is to describe a method of calculating the intensity of a gas laser which is applicable at high intensities and to compare the results of the calculation to experimental data obtained using a 1.15-μm He-Ne laser.

Section II describes how the laser intensity is related to the macroscopic polarization of the gas. In Sec. III, the quantum-mechanical description of the atoms is developed, resulting in equations for the time-dependent components of the density matrix. The solution to these equations in the form of a Fourier series is developed, and the macroscopic polarization is related to the coefficients of the Fourier series. Section IV is a description of the method used to find the coefficients. In Sec. V, the laser intensity is calculated for both flat and Maxwellian velocity distributions. Section VI is a calculation of the effects of Lorentz collision broadening on laser characteristics. In Sec. VII, the results of the calculation are compared with experimental data from a 1.15-μm He-Ne laser.

II. POLARIZATION OF MEDIUM

Lamb[1] has shown that the calculation of laser characteristics reduces to the calculation of the macroscopic polarization of the medium by the laser field. In the present work, the electric field is assumed to be in the x direction and of magnitude

$$\mathcal{E}(z, t) = E\cos(\nu t+\varphi)\sin Kz\,, \tag{1}$$

where the z direction is along the laser axis. If L is the cavity length, then $K = n\pi/L$, where n is a large integer. The amplitude E and the phase φ of the field are slowly varying functions of time; for the present purposes, they may be assumed to be constant.

The electric field acting on the gas atoms induces a macroscopic electric polarization $P(z, t)$, with the space Fourier component

$$P(t) = (2/L)\int_0^L P(z, t)\sin Kz\,dz$$

$$\equiv C\cos(\nu t+\varphi)+S\sin(\nu t+\varphi)\,. \tag{2}$$

The equation for the amplitude of the electric field is[1]

$$\dot{E}+\tfrac{1}{2}(\nu/Q)E = -\tfrac{1}{2}(\nu/\epsilon_0)S\,, \tag{3}$$

where Q is the "Q" of the cavity. (A similar equation relates the frequency of the laser light to the coefficient C.) A steady state exists when $\dot{E} = 0$, i.e.,

$$S/E = -\epsilon_0/Q = \text{const.} \tag{4}$$

This equation is analogous to the "gain" = "loss" equation used by Bennett.[2]

In Lamb's "third-order" theory, we have

$$S = g_1 E - g_3 E^3\,, \tag{5}$$

where g_1 and g_3 are functions of the cavity length and of atomic parameters but not of E. The laser intensity, proportional to E^2, is then the solution to

$$S/E = g_1 - g_3 E^2 = \text{const.} \tag{6}$$

As Lamb points out, this solution is only applicable at very low laser intensities. However, it was not possible to tell at just what intensity his theory becomes inaccurate.

In the present method, S/E as a function of E^2 is obtained without using an expansion in E^2. The laser intensity is still given by solving Eq. (4) for E^2, but S/E is no longer a series in powers of E^2.

III. DENSITY-MATRIX EQUATIONS

The gas atoms comprising the medium are thought of as having two excited levels a and b which are connected by electric dipole transitions. The wave function describing an atom is

$$\psi = a(t)\psi_a + b(t)\psi_b\,, \tag{7}$$

where $a(t)$ and $b(t)$ are the amplitudes of levels a and b, respectively. From the time-dependent Schrödinger equation

$$i\hbar\frac{d\psi}{dt} = H\psi = [H_0 + e\,\mathcal{E}(t)x]\psi\,, \tag{8}$$

follow the equations for the amplitudes:

$$\dot{a} = -ia E_a/\hbar - ib V_{ab} - \tfrac{1}{2}\gamma_a a, \tag{9}$$

$$\dot{b} = -ib E_b/\hbar - ia V_{ab}^* - \tfrac{1}{2}\gamma_b b, \tag{10}$$

where E_a and E_b are the energies of states a and b,

$$V_{ab} = -\frac{\mathcal{P}\mathcal{E}(z,t)}{\hbar} = -\left(\frac{\mathcal{P}E}{\hbar}\right)\cos(\nu t+\varphi)\sin Kz, \tag{11}$$

and $$\mathcal{P} = -e\int \psi_a^* x \psi_b \, d\tau. \tag{12}$$

The terms $-(\frac{1}{2}\gamma_a)a$ and $-(\frac{1}{2}\gamma_b)b$ have been added to account for the spontaneous decay of levels a and b to other levels. The lifetimes of levels a and b are $1/\gamma_a$ and $1/\gamma_b$, respectively.

The equations describing the time behavior of the density-matrix components of a single atom follow directly from Eqs. (9) and (10):

$$\dot{\rho}_{aa} \equiv \frac{d}{dt}(aa^*) = -\gamma_a \rho_{aa} + 2\,\mathrm{Re}(iV_{ab}^*\rho_{ab}), \tag{13}$$

$$\dot{\rho}_{bb} \equiv \frac{d}{dt}(bb^*) = -\gamma_b \rho_{bb} - 2\,\mathrm{Re}(iV_{ab}^*\rho_{ab}), \tag{14}$$

$$\dot{\rho}_{ab} \equiv \frac{d}{dt}(ab^*) = -(\gamma_{ab}+i\omega_{ab})\rho_{ab} + iV_{ab}(\rho_{aa}-\rho_{bb}), \tag{15}$$

where $\gamma_{ab} \equiv \frac{1}{2}(\gamma_a+\gamma_b)$ and $\omega_{ab} \equiv (E_a - E_b)/\hbar$. The dipole moment per unit volume due to one atom at position z at time t is

$$-\int \psi^* e x \psi \, d\tau = -e(a^*b\int \psi_a^* x \psi_b d\tau + ab^* \int \psi_b^* x \psi_a d\tau)$$
$$= 2\,\mathrm{Re}(\rho_{ab}\mathcal{P}^*). \tag{16}$$

The macroscopic polarization $P(z, t)$ is gotten by summing this expression over all atoms which happen to be at z at time t.

Lamb[1] and Stenholm and Lamb[6] consider atoms excited to a given state $i = a$ or b at time t_0 and position z_0 which arrive at z at time t. The atoms are assumed to have uniform speeds in the axial direction v_z so that z, t is related to z_0, t_0 by

$$z = z_0 + v_z(t - t_0). \tag{17}$$

They calculate the polarization due to these atoms [Eq. (16)] and then integrate the resulting expression over z_0, t_0, i, and v_z to obtain the macroscopic polarization at z, t.

In the present method, the density-matrix components are taken as describing a volume of atoms moving along the z axis with speed v_z. Excitation is accounted for by adding terms λ_a and λ_b to $\dot{\rho}_{aa}$ and $\dot{\rho}_{bb}$, respectively, where λ_i is the number of atoms per cm^3 sec excited to state i with speed v_z; λ_i is assumed to be a function of v_z but not of z or t. As the atoms move through the standing-wave pattern, they experience a potential which is changing in time not only because of the $\cos(\nu t+\varphi)$ term in V_{ab} but also because of the $\sin Kz$ term, since their position z changes in time. If the atoms pass through the position $\bar{z}$ at time $\bar{t}$, then their position at time t is

$$z = \bar{z} + v_z(t - \bar{t}). \tag{18}$$

Using Eq. (11) and the rotating wave approximation, [1]

$$V_{ab} = -\left(\frac{\mathcal{P}E}{4i\hbar}\right)e^{-i(\nu t+\varphi)}(e^{iKz} - e^{-iKz})$$
$$= -\left(\frac{\mathcal{P}E}{4i\hbar}\right)e^{-i\varphi}[e^{iK(\bar{z}-v_z\bar{t})}e^{-i(\nu-Kv_z)t}$$
$$- e^{-iK(\bar{z}-v_z\bar{t})}e^{-i(\nu+Kv_z)t}]. \tag{19}$$

The latter expression shows explicitly the two frequencies $\nu - Kv_z$ and $\nu + Kv_z$ of the two travelling waves comprising the standing wave, as well as the phase relationship between them.

The problem is solved first for fixed v_z, $\bar{z}$, and $\bar{t}$; z and t are then dependent variables. The final result is to be summed over v_z, $\bar{z}$, and $\bar{t}$, although the result turns out to be independent of $\bar{z}$ and $\bar{t}$, so that only a summing over v_z is necessary. (One could choose $\bar{z}$, $\bar{t}$ to be z_0, t_0 the excitation point; the final result then turns out to be independent of z_0, t_0, as one would expect for a steady-state problem such as this one.)

Thus, the density-matrix component equations used here are

$$\dot{\rho}_{aa} = \lambda_a - \gamma_a\rho_{aa}$$
$$- 2\,\mathrm{Re}\left[\left(\frac{\mathcal{P}^*E}{4\hbar}\right)e^{i(\nu t+\varphi)}(e^{iKz} - e^{-iKz})\rho_{ab}\right], \tag{20}$$

$$\dot{\rho}_{bb} = \lambda_b - \gamma_b\rho_{bb}$$
$$+ 2\,\mathrm{Re}\left[\left(\frac{\mathcal{P}^*E}{4\hbar}\right)e^{i(\nu t+\varphi)}(e^{iKz} - e^{-iKz})\rho_{ab}\right], \tag{21}$$

$$\dot{\rho}_{ab} = -(\gamma_{ab}+i\omega_{ab})\rho_{ab}$$
$$-\left(\frac{\mathcal{P}E}{4\hbar}\right)e^{-i(\nu t+\varphi)}(e^{iKz} - e^{-iKz})(\rho_{aa}-\rho_{bb}). \tag{22}$$

After substituting

$$\rho_{ab} = \left(\frac{\mathcal{P}E}{4\hbar}\right)e^{-i(\nu t+\varphi)}f_{ab},$$

the equations become

$$\dot{\rho}_{aa} = \lambda_a - \gamma_a\rho_{aa} - \left(\frac{|\mathcal{P}|^2E^2}{8\hbar^2}\right)\mathrm{Re}[(e^{iKz} - e^{-iKz})f_{ab}], \tag{23}$$

$$\dot{\rho}_{bb} = \lambda_b - \gamma_b\rho_{bb} + \left(\frac{|\mathcal{P}|^2E^2}{8\hbar^2}\right)\mathrm{Re}[(e^{iKz} - e^{-iKz})f_{ab}], \tag{24}$$

$$\dot{f}_{ab} - i(\nu - \omega_{ab} + i\gamma_{ab})f_{ab} = -(e^{iKz} - e^{-iKz})(\rho_{aa}-\rho_{bb}). \tag{25}$$

The solution to Eqs. (23)–(25) is obtained by

assuming a series in odd powers of e^{iKz} for f_{ab} and series in even powers of e^{iKz} for ρ_{aa} and ρ_{bb}, all with undetermined coefficients. The coefficients are gotten by equating powers of e^{iKz} in Eqs. (23)–(25). The result is

$$\rho_{aa}-\rho_{bb}=n_0\left\{1-2\alpha\,\mathrm{Re}(B_0R_0)+2\alpha\,\mathrm{Re}\left[\sum_{n=1}^{\infty}(B_{n-1}R_{n-1}-B_nR_n)p_ne^{2niKz}\right]\right\}, \tag{26}$$

$$\rho_{ab}=-i\left(\frac{\mathcal{P}E}{4\hbar}\right)n_0e^{-i(\nu t+\varphi)}\times\left[\sum_{n=0}^{\infty}\left(\frac{B_n}{\Delta_n^-}E^{(2n+1)iKz}-\frac{B_n^*}{\Delta_n^+}e^{-(2n+1)iKz}\right)\right], \tag{27}$$

where $n_0\equiv\lambda_a/\gamma_a-\lambda_b/\gamma_b$, $\alpha\equiv|\mathcal{P}|^2E^2/8\hbar^2\gamma_a\gamma_b$,

$$\Delta_n^{\pm}\equiv\nu-\omega_{ab}\pm(2n+1)Kv_z+i\gamma_{ab},$$

$$R_n\equiv i\gamma_{ab}\left(\frac{1}{(\Delta_n^-)}-\frac{1}{(\Delta_n^+)^*}\right),$$

$$p_n\equiv-\frac{i\gamma_a\gamma_b}{4\gamma_{ab}}\left(\frac{1}{nKv_z-\frac{1}{2}i\gamma_a}+\frac{1}{nKv_z-\frac{1}{2}i\gamma_b}\right),$$

and the coefficients B_n obey the recursion relations

$$B_0=1-\alpha[2\,\mathrm{Re}(B_0R_0)+(B_0R_0-B_1R_1)p_1], \tag{28}$$

$$B_n=\alpha[B_{n+1}R_{n+1}p_{n+1}-B_nR_n(p_n+p_{n+1})+B_{n-1}R_{n-1}p_n],\quad n>0. \tag{29}$$

The quantity n_0 is the unperturbed inversion density at v_z. Defining

$$\lambda_i=\Lambda_iW(v_z),$$

where Λ_i is the number of atoms excited to state i per $\mathrm{cm}^3\,\mathrm{sec}$, and

$$\int_{-\infty}^{\infty}W(v_z)dv_z\equiv1\ ,$$

then $$n_0=\left(\frac{\Lambda_a}{\gamma_a}-\frac{\Lambda_b}{\gamma_b}\right)W(v_z)=NW(v_z),$$

where N is the unperturbed total inversion density

$$\int_{-\infty}^{\infty}n_0\,dv_z=N.$$

The saturation parameter α is proportional to the intensity of the laser field and inversely proportional to the level widths. α is of the order of the ratio of the stimulated transition probability per second to the spontaneous transition probability per second at resonance. The present calculation is applicable at large values of α, whereas the iterative approach is applicable only for small α. α is large even at moderate intensities if the level widths are small.

The quantities R_n and p_n are defined in such a way that, in an integration over v_z, the poles are all above the real axis, for example,

$$\int_{-\infty}^{\infty}R_mR_n\,dv_z=\int_{-\infty}^{\infty}R_mp_n\,dv_z=0,$$

$$\int_{-\infty}^{\infty}R_mR_n^*\,dv_z\neq0\ .$$

The macroscopic polarization at z, t due to atoms with v_z is

$$P_{v_z}(z,t)=2\,\mathrm{Re}(\rho_{ab}\mathcal{P}^*)=-\frac{|\mathcal{P}|^2E}{2\hbar}n_0\times\mathrm{Re}\left\{ie^{-i(\nu t+\varphi)}\left[\sum_0^{\infty}\left(\frac{B_n}{\Delta_n^-}e^{(2n+1)iKz}-\frac{B_n^*}{\Delta_n^+}e^{-(2n+1)iKz}\right)\right]\right\}. \tag{30}$$

To calculate the laser intensity, one needs the coefficient of $\sin Kz$ [Eq. (2)]:

$$P_{v_z}(t)=\frac{2}{L}\int_0^LP_{v_z}(z,t)\sin Kz\,dz=-\frac{|\mathcal{P}|^2E}{2\hbar}n_0\,\mathrm{Re}\left[ie^{-i(\nu t+\varphi)}\left(\frac{iB_0}{\Delta_0^-}+\frac{iB_0^*}{\Delta_0^+}\right)\right]\equiv C_{v_z}\cos(\nu t+\varphi)+S_{v_z}\sin(\nu t+\varphi). \tag{31}$$

Thus, the out-of-phase component of the macroscopic polarization due to atoms with v_z is

$$S_{v_z}=-\frac{|\mathcal{P}|^2E}{2\hbar}n_0\,\mathrm{Re}\left[i\left(\frac{B_0}{\Delta_0^-}+\frac{B_0^*}{\Delta_0^+}\right)\right]=-\frac{|\mathcal{P}|^2E}{2\hbar}n_0\,\mathrm{Re}\left[iB_0\left(\frac{1}{\Delta_0^-}-\frac{1}{(\Delta_0^+)^*}\right)\right]=-\frac{|\mathcal{P}|^2E}{2\hbar\gamma_{ab}}n_0\,\mathrm{Re}(B_0R_0)=-\frac{|\mathcal{P}|^2E}{2\hbar\gamma_{ab}}n_0G, \tag{32}$$

where

$$G=G(v_z,\alpha,\nu-\omega_{ab},\gamma_{ab},\gamma_a,\gamma_b)\equiv\mathrm{Re}(B_0R_0). \tag{33}$$

To integrate over velocities, replace n_0 by $NW(v_z)$. Then

$$S=\int_{-\infty}^{\infty}S_{v_z}\,dv_z=-\frac{|\mathcal{P}|^2EN}{2\hbar\gamma_{ab}}\int_{-\infty}^{\infty}G(v_z)W(v_z)\,dv_z=-\frac{|\mathcal{P}|^2EN}{2\hbar\gamma_{ab}}J, \tag{34}$$

where $$J=J(\alpha,\nu-\omega_{ab},\gamma_{ab},\gamma_a,\gamma_b)\equiv\int_{-\infty}^{\infty}G(v_z)W(v_z)\,dv_z. \tag{35}$$

By using the recursion relations, one can show that $B_0(-v_z)=B_0^*(v_z)$. Also, $R_0(-v_z)=R_0^*(v_z)$. Therefore, if $W(v_z)$ is symmetric about $v_z=0$,

$$J=2\int_0^{\infty}G(v_z)W(v_z)\,dv_z. \tag{36}$$

For a Maxwellian velocity distribution, we have

$$J=\frac{2}{\sqrt{\pi}}\int_0^\infty G(v_z)\,e^{-(v_z/u)^2}\,\frac{dv_z}{u}. \tag{37}$$

The laser intensity parameter α is determined by

$$S/E=-\epsilon_0/Q=\text{const.} \tag{4}$$

Suppose N_T is the threshold inversion density at $\nu=\omega_{ab}$, N_T is proportional to the cavity losses, then Eq. (4) can be expressed in the form

$$-\frac{|\mathcal{P}|^2N}{2\hbar\gamma_{ab}}J(\alpha,\nu-\omega_{ab},\gamma_{ab},\gamma_a,\gamma_b)$$

$$=-\frac{|\mathcal{P}|^2N_T}{2\hbar\gamma_{ab}}J(0,0,\gamma_{ab},\gamma_a,\gamma_b), \tag{38}$$

$$\text{or}\quad J/J_T=N_T/N\equiv\mathfrak{N}^{-1}, \tag{39}$$

where $J_T\equiv J(0,0,\gamma_{ab},\gamma_a,\gamma_b)$. α is then the solution to Eq. (39). Since Eq. (39) is analogous to a gain = loss equation, it is evident that $G(v_z)$ is analogous to the gain due to atoms with velocity v_z.

IV. DETERMINATION OF COEFFICIENTS OF FOURIER SERIES

In order to calculate the laser intensity, the recursion equations [Eqs. (28) and (29)] must be solved for B_0. One method is the iterative method. Solving the equations iteratively for B_0 can be shown to be equivalent to solving the original density-matrix component equations [Eqs. (20)–(22)] iteratively. In Appendix A, the iterative solution is derived and

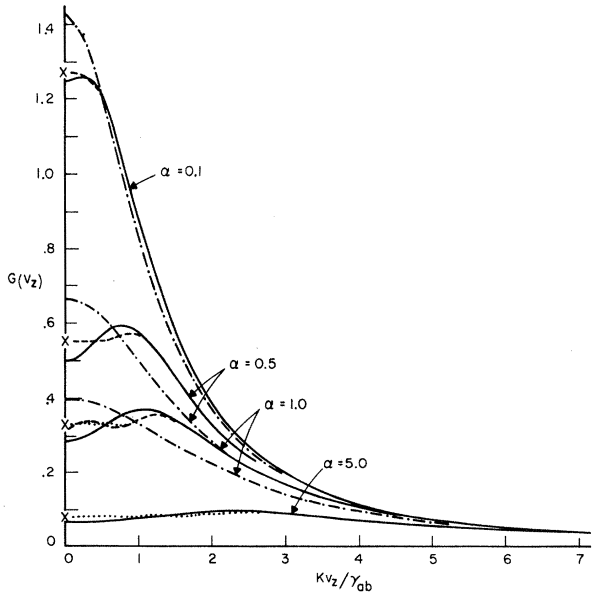

FIG. 1. $G(v_z)=\mathrm{Re}(B_0R_0)$ as a function of Kv_z/γ_{ab} for $\nu-\omega_{ab}=0$, $\gamma_a=\gamma_b$. The solid lines are case A; the dashed lines are case B; the dotted lines are case C; and the dot-dashed lines are for $B_0=1/(1+2\alpha\,\mathrm{Re}\,R_0)$. The exact solutions for $v_z=0$ are denoted by x.

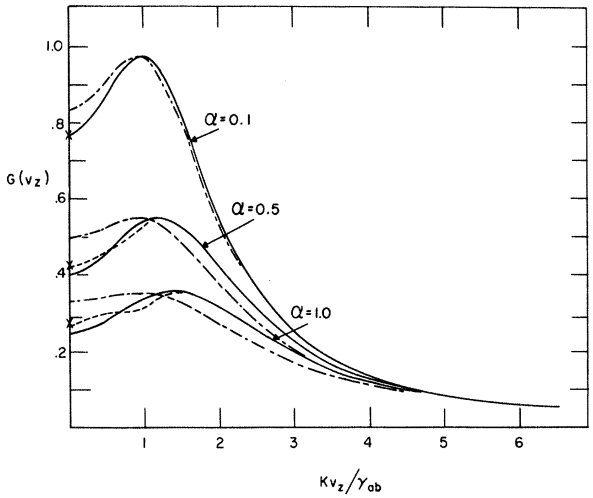

FIG. 2. $G(v_z)=\mathrm{Re}(B_0R_0)$ as a function of Kv_z/γ_{ab} for $\nu-\omega_{ab}=\gamma_{ab}$, $\gamma_a=\gamma_b$. The solid lines are case A; the dashed lines are case B; the dot-dashed lines are for $B_0=1/(1+2\alpha\mathrm{Re}R_0)$. For $\alpha=0.1$, cases B and C coincide with case A. Case C coincides with case B for all the α's. The x's are the exact solutions for $v_z=0$.

is shown to lead to Lamb's first-order and third-order results.[1] The solution is carried to fifth order to show that the series appears to be asymptotic and thus is not useful except at small values of α. For this reason, another solution to the recursion relations is desired.

In Appendix B it is shown that there are two Fourier series for ρ_{ab}, a divergent one and a convergent one. The convergence condition is

$$\lim\frac{B_n}{B_{n-1}}<1,\quad\text{as}\quad n\to\infty.$$

For $v_z\neq0$, the desired convergent solution has the property

$$\lim\frac{B_n}{B_{n-1}}=0,\quad\text{as}\quad n\to\infty.$$

In Appendix C, the recursion equations are solved exactly for the case $v_z=0$, as a check on the method. If $v_z\neq0$, no exact solution is available, but a solution can be obtained to arbitrary accuracy by means of the following procedure: Set B_n equal to zero for all n greater than some N. Then solve for B_N, B_{N-1}, B_{N-2}, $\cdots$, and eventually for B_0. The accuracy of this procedure can be judged by doing the calculation for N and then for $N+1$ and comparing the results. If no change results in going from N to $N+1$, then the solution obtained starting at N is good enough.

An examination of the recursion equations shows that the quantities B_1, B_2, $\cdots$, p_1, p_2, $\cdots$, influence the results only for certain values of α, $\nu-\omega_{ab}$, and v_z. Since $B_1\to0$ as $\alpha\to0$, the effect of

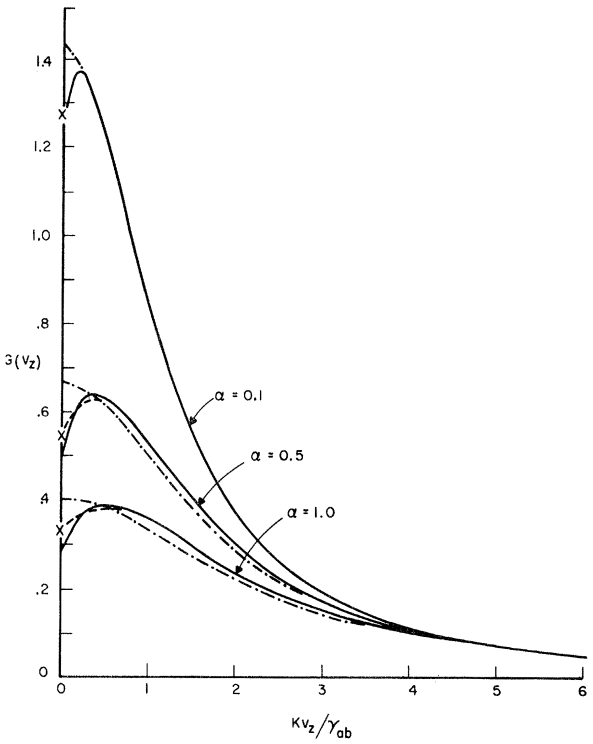

FIG. 3. $G(v_z) = \mathrm{Re}(B_0 R_0)$ as a function of Kv_z/γ_{ab} for $\nu - \omega_{ab} = 0$, $\gamma_a = 10\,\gamma_b$ or $\gamma_b = 10\,\gamma_a$. The solid lines are case A; the dashed lines are cases B and C; and the dot-dashed lines are for $B_0 = 1/(1 + 2\alpha\,\mathrm{Re}R_0)$. Cases A and B coincide for $\alpha = 0.1$. The x's are the exact solutions for $v_z = 0$.

a nonzero B_1 on the value of B_0 increases as α increases.

If $|\nu - \omega_{ab}|$ is large compared to γ_{ab}, the term $(B_0 R_0 - B_1 R_1)p_1$ in the expression for B_0 is small for all v_z, since p_1 has its maximum at $v_z = 0$, while R_0 and R_1 peak at $Kv_z = \pm\,|\nu - \omega_{ab}|$ and $\pm\frac{1}{3}|\nu - \omega_{ab}|$, respectively. Then B_0 is the solution to

$$B_0 \cong 1 - \alpha[2\,\mathrm{Re}(B_0 R_0)]$$

or

$$B_0 \cong [1 + \alpha(R_0 + R_0^*)]^{-1} = \left[1 + 2\alpha\left(\frac{\gamma_{ab}^2}{(\nu - \omega_{ab} - Kv_z)^2 + \gamma_{ab}^2} + \frac{\gamma_{ab}^2}{(\nu - \omega_{ab} + Kv_z)^2 + \gamma_{ab}^2}\right)\right]^{-1}. \quad (40)$$

This is equivalent to the results of Refs. 4 and 5 and is also contained in Ref. 1.

Even if $|\nu - \omega_{ab}|$ is comparable to γ_{ab}, B_0 is given by Eq. (40) except near $v_z = 0$, since p_1 is small everywhere else. Similarly, B_1, B_2, $\cdots$ are small except near $v_z = 0$, because of their dependence on p_1, p_2, $\cdots$.

Figures 1–4 show $G(v_z) = \mathrm{Re}(B_0 R_0)$ as a function of Kv_z/γ_{ab} for several values of $\nu - \omega_{ab}$ and γ_a/γ_b. Case A is the solution obtained by setting $B_1 = B_2 = \cdots = 0$, case B that obtained for $B_2 = B_3 \cdots = 0$, and case C the solution for $B_3 = B_4 = \cdots = 0$. Explicit expressions for $G(v_z)$ in the various cases are contained in Appendix D. $G(v_z)$ is symmetric about $v_z = 0$. For case A, B_0 is the solution to

$$B_0 = 1 - \alpha[2\,\mathrm{Re}(B_0 R_0) + B_0 R_0 p_1];$$

it differs from Eq. (40) (and from Refs. 4 and 5) by the term $\alpha B_0 R_0 p_1$. The figures show that case A is worst for $\gamma_a = \gamma_b$, for $\nu = \omega_{ab}$, for large α and for $v_z = 0$. In Fig. 1, the dip in $G(v_z)$ near $v_z = 0$ (see also Ref. 6), most pronounced for unequal γ_a and γ_b, is caused by the term $B_0 R_0 p_1$. This effect is not taken into account in Bennett's hole-burning theory[2] or in other theories where the response of the atoms to the electromagnetic field is assumed to depend on γ_{ab} only, and not on γ_a and γ_b.

Although there are noticeable differences among cases A, B, and C in Figs. 1–4, these differences do not affect the results for the laser intensity very much, at least in the case of a flat velocity distribution, since J/J_T is proportional to the areas under the curves of $G(v_z)$ versus v_z, which are not very different for the three different approximations. This point illustrated in Fig. 5, where J/J_T is plotted against α for $\gamma_a = \gamma_b$, and for $(\nu - \omega_{ab})/\gamma_{ab} = 0$, 2, and 4, for a flat velocity distribution; the difference between cases A and B is only about 2% (and the corresponding error in α is also about 2%) at $\alpha = 5$, $\nu - \omega_{ab} = 0$. The error

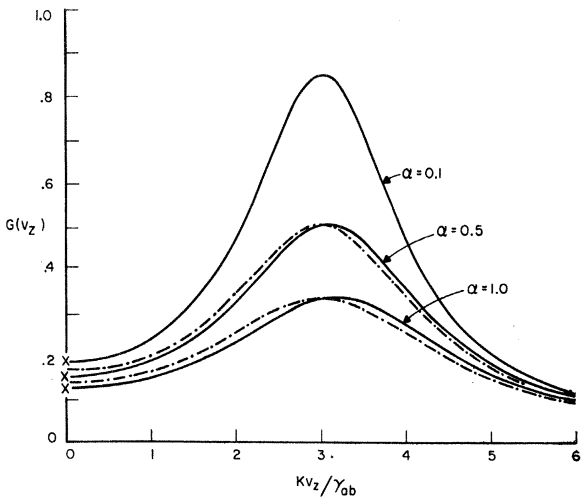

FIG. 4. $G(v_z) = \mathrm{Re}(B_0 R_0)$ as a function of Kv_z/γ_{ab} for $\nu - \omega_{ab} = 3\gamma_{ab}$, $\gamma_a = \gamma_b$. The solid lines are cases A, B, and C; the dot-dashed lines are for $B_0 = 1/(1 + 2\alpha\,\mathrm{Re}R_0)$; and the x's are the exact solutions for $v_z = 0$.

for $\nu - \omega_{ab} > 0$ is much smaller. Since the rest of the paper is concerned with values of α much smaller than 5, case A only will be used in what follows. However, one can easily extend the results to higher α simply by using cases B, C, etc. (see Appendix D).

Figures 1–5 also show $G(v_z)$ and J/J_T calculated using $B_0 = 1/(1 + 2\alpha R_e R_0)$ [Eq. (40)]. The errors in α associated with this approximation are of the order of 10% at $\alpha \sim 0.1 \rightarrow 1.0$ for a flat velocity distribution and are larger for a Maxwellian distribution where the effects of zero-velocity atoms are more important. Figure 15 shows J/J_T as a function of α for the third- and fifth-order iterative solutions; the scale of α has been expanded, since these solutions are meant to be applicable only at small values of α. Figure 15 shows that both iterative solutions are in error by about 20% in α at $\alpha = 0.05$ (or at $I = 0.2$ where I is the intensity parameter of Ref. 1).

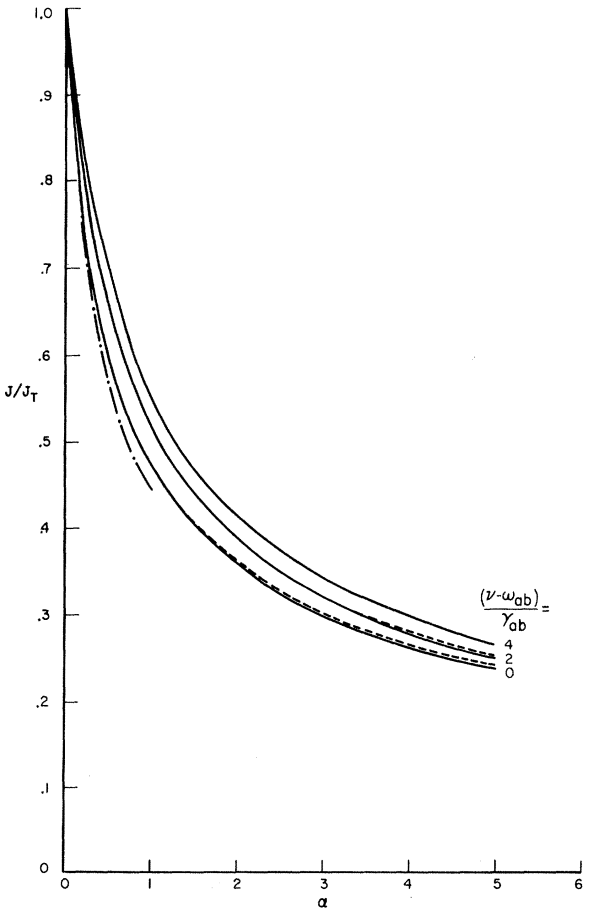

FIG. 5. J/J_T as a function of α and $(\nu - \omega_{ab})/\gamma_{ab}$ for a flat velocity distribution and $\gamma_a = \gamma_b$. The solid lines are for case A, the dashed lines for cases B and C, and the dot-dashed lines for $B_0 = 1/(1 + 2\alpha\, \mathrm{Re} R_0)$. Cases B and C coincide for $(\nu - \omega_{ab})/\gamma_{ab} = 4$.

V. LASER INTENSITY

A. Intensity for Case of Flat Velocity Distribution

The method used to calculate the laser intensity is to calculate J/J_T as a function of α (on a computer), draw curves such as those in Fig. 5, draw a horizontal line representing $J/J_T = \mathfrak{N}^{-1}$, and find α as a function of $\nu - \omega_{ab}$ from the intersections of the horizontal line with the J/J_T curves for different values of $\nu - \omega_{ab}$. (Of course, if one had a great deal of computer time available, α could be found as a function of $\nu - \omega_{ab}$ and $\mathfrak{N}^{-1}$ without the use of graphs.) Typical results of such a calculation are shown in Fig. 6. Also shown is the third-order iterative solution for a flat velocity distribution

$$\alpha = \frac{(1 - \mathfrak{N}^{-1})}{1 + \gamma_{ab}^2/[(\nu - \omega_{ab})^2 + \gamma_{ab}^2]} .$$

This is equivalent to Lamb's third-order solution or to Bennett's hole-burning result; the accuracy is quite poor for $\mathfrak{N}^{-1}$ smaller than about 0.9, or for α greater than about 0.05 at $\nu - \omega_{ab} = 0$.

For single-mode operation over the entire tuning curve, a typical 30-cm-long 1.15-μm He-Ne laser has $\mathfrak{N}^{-1}$ greater than about 0.8. For a 30-cm 0.6328-μm laser, $\mathfrak{N}^{-1}$ is greater than about 0.9 for single-mode operation. Of course, $\mathfrak{N}^{-1}$ can become quite a bit smaller than these values for shorter lasers and longer wavelengths, for 3.39-μm lasers, for example.

The quantity $\alpha(\nu - \omega_{ab} \rightarrow \infty) \equiv \alpha_\infty$ is also shown in Fig. 6. It was obtained from the solution for large $(\nu - \omega_{ab})/\gamma_{ab}$:

$$B_0 = \frac{1}{1 + 2\alpha\, \mathrm{Re}\, R_0} ,$$

which can be integrated analytically by contour integration with the following results: If the condition

$$\alpha^2 \ll [(\nu - \omega_{ab})/\gamma_{ab}]^2 (1 + 2\alpha)$$

is fulfilled, then, for large $(\nu - \omega_{ab})/\gamma_{ab}$

$$\frac{J}{J_T} \cong (1 + 2\alpha)^{1/2} \left[1 - \alpha\left(\frac{\gamma_{ab}^2}{(\nu - \omega_{ab})^2 + \gamma_{ab}^2(1 + 2\alpha)}\right)\right] .$$

Thus, $\lim \dfrac{J}{J_T} = \dfrac{1}{\sqrt{(1 + 2\alpha)}}$, as $|\nu - \omega_{ab}| \rightarrow \infty$.

The condition $J/J_T = \mathfrak{N}^{-1}$ gives

$$\lim \alpha = \tfrac{1}{2}(\mathfrak{N}^2 - 1) \equiv \alpha_\infty, \text{ as } |\nu - \omega_{ab}| \rightarrow \infty .$$

Figure 7(a) shows the width of the dip, the full width at $\alpha = \frac{1}{2}(\alpha_\infty - \alpha_0)$ in units of $(\nu - \omega_{ab})/\gamma_{ab}$, as a function of $\mathfrak{N}$. α_0 is $\alpha(\nu - \omega_{ab} = 0)$. Figure 7(b) shows α_∞ and α_0 as functions of $\mathfrak{N}$. The points in Fig. 7 were obtained from graphs similar to Fig 6.

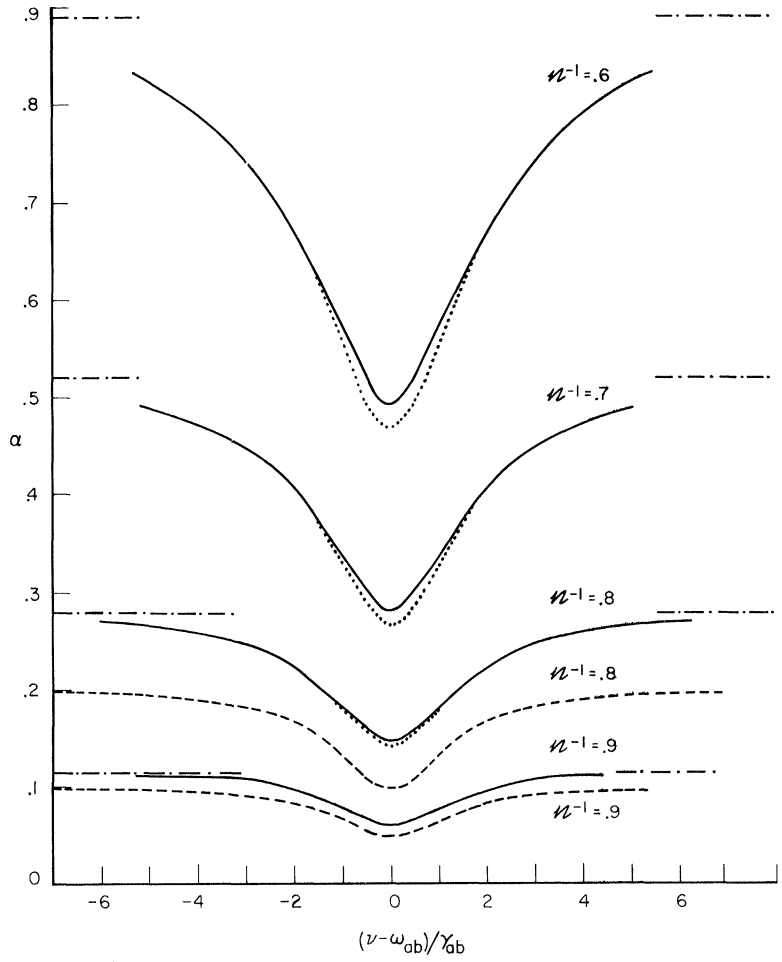

FIG. 6. The intensity parameter α as a function of $(\nu-\omega_{ab})/\gamma_{ab}$ calculated for a flat velocity distribution. The dashed lines represent the third-order iterative solution for $\mathfrak{N}^{-1}=0.8$ and 0.9. The other lines represent results of the present work (cases A, B, or C, which coincide for these low values of α). The solid lines are for $\gamma_a=\gamma_b$; the dotted lines are the $\gamma_a=10\gamma_b$ or $\gamma_b=10\gamma_a$; and the dot-dashed lines represent $\alpha(\nu-\omega_{ab}\to\infty)$.

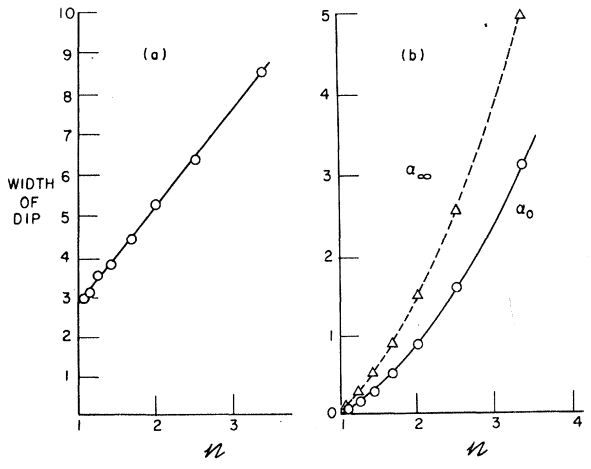

FIG. 7. (a) The calculated width of the dip in α versus $(\nu-\omega_{ab})/\gamma_{ab}$ as a function of $\mathfrak{N}$, for $\gamma_a=\gamma_b$. The width is in units of $(\nu-\omega_{ab})/\gamma_{ab}$. (b) α_∞ and α_0 as a function of $\mathfrak{N}$. (The points in Fig. 7 were obtained from the curves in Fig. 6 and similar curves for larger α.)

B. Intensity for Case of Maxwellian Velocity Distribution

For a flat velocity distribution, J/J_T is a function of α, $(\nu-\omega_{ab})/\gamma_{ab}$, and the ratio of γ_b to γ_a. For a Maxwellian distribution, J/J_T is a function of these quantities and also of η, where

$$\eta\equiv\gamma_{ab}/Ku \tag{41}$$

[see Eq. (37)]. The functions determining $G(v_z)$ $=\mathrm{Re}(B_0R_0)$ peak at $Kv_z=0$ (the p_n's) and Kv_z $=\pm|(\nu-\omega_{ab})/(2n+1)|$ (the R_n's). However, if $|\nu-\omega_{ab}|$ is large, we have already seen that only R_0 is important in determining B_0; R_0 peaks at $Kv_z=\pm|\nu-\omega_{ab}|$, with a sharpness which is determined by γ_{ab}. If η is much smaller than 1 (the "Doppler limit"), then R_0 peaks very sharply compared to changes in the velocity function, and $e^{-(vz/u)^2}$ can be replaced by $\exp\{-[(\nu-\omega_{ab})/Ku]^2\}$ $=e^{-\xi^2}$, where

$$\xi\equiv(\nu-\omega_{ab})/Ku. \tag{42}$$

Then $e^{-\xi^2}$ can be taken outside the integral of Eq.

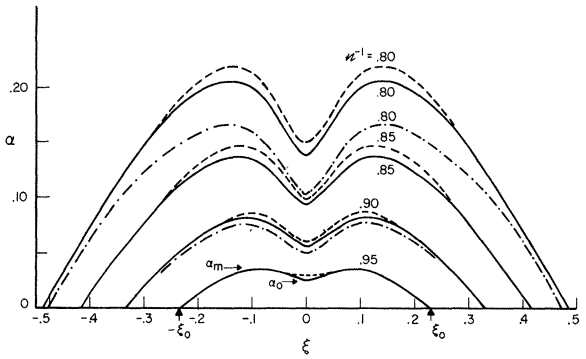

FIG. 8. The intensity parameter α as a function of $\xi = (\nu - \omega_{ab})/Ku$, for a Maxwellian velocity distribution. Here, $\eta(\equiv \gamma_{ab}/Ku) = 0.05$. The solid curves are the present results; the dashed curves represent the present work in the Doppler limit, and the dot-dashed curves are from the third-order iterative solution, Eq. (76), for $\mathfrak{N}^{-1} = 0.8$ and 0.9 only.

(68) and

$$J/J_T \cong e^{-\xi^2} (J/J_T)_{\text{flat}} . \tag{43}$$

Here, $(J/J_T)_{\text{flat}}$ is $J/J/_T$ calculated for a flat velocity distribution.

The Doppler-limit approximation becomes worse near $\nu - \omega_{ab} = 0$, because there functions peaking both at $Kv_z = 0$ and at $Kv_z = \pm\,|(\nu - \omega_{ab})/(2n+1)|$ are important in determining B_0. It turns out not to be very good even for $\eta = 0.05$, so that the integration over velocity in Eq. (37) had to be done numerically. Typical results of such a calculation are shown in Fig. 8 for $\eta = 0.05$, $\gamma_a = \gamma_b$. The main purpose of this calculation was to obtain results to compare with experimental data taken for $\mathfrak{N}^{-1}$ greater than 0.8; Fig. 6 shows that the intensity is not sensitive to the ratio of γ_b to γ_a in this region, so no attempt was made to vary the ratio in doing the Maxwellian calculation.

Also shown in Fig. 8 is the Doppler-limit case, Eq. (43), and the third-order iterative solution in the Doppler limit,

$$\alpha = \alpha_L = \frac{1 - \mathfrak{N}^{-1} e^{[(\nu-\omega_{ab})/Ku]^2}}{1 + \gamma_{ab}^2/[(\nu-\omega_{ab})^2 + \gamma_{ab}^2]} = \frac{1 - \mathfrak{N}^{-1} e^{\xi^2}}{1 + \eta^2/(\xi^2+\eta^2)} \tag{44}$$

(see Appendix A). α_L, or the function

$$\alpha_L' = \frac{e^{-\xi^2} - \mathfrak{N}^{-1}}{1 + \eta^2/(\xi^2+\eta^2)} ,$$

which is equivalent to α_L at low intensities, is the intensity function of Refs. 1 and 2. Although Eq. (44) was not meant to be applicable except at very low intensities, [1] its range of applicability has not been clear. Since Eq. (44) has been used extensively in the analysis of experimental data, it seems useful to compare quantities calculated using α_L with ones otten using the present method to show the range o. oplicability of α_L. This is done in the following paragraphs.

For purposes of comparing theoretical and experimental results, the following quantities were defined: α_m, the maximum of the intensity curve; α_0, the value of α at $\nu - \omega_{ab} = 0$; and ξ_0, the value of ξ for which $\alpha = 0$ (see Fig. 8). ξ_0^2 is in some respects a measure of the inversion density; in Eq. (44), $\alpha = 0$ at $e^{\xi_0^2} = \mathfrak{N}$. For small ξ_0^2, $\xi_0^2 \cong \mathfrak{N} - 1$. Of course, the exact relationship between ξ_0^2 and $\mathfrak{N}$ can be found from curves such as those in Fig. 8, but it is simpler to use ξ_0^2 as a parameter, since ξ_0 can be measured experimentally.

The quantity α_m/α_0 is plotted against ξ_0^2 in Fig. 9. The quantity $(\alpha_m/\alpha_0) - 1$ is equal to the depth of the "Lamb dip" divided by the height at the center of the tuning curve and is a useful parameter for comparison with experiment. The values of α_m/α_0 were obtained from curves similar to the intensity curves of Fig. 8, calculated for different values of η. The indicated errors are caused by the graphical methods used and not by errors in the calculated values of J/J_T; the error could be reduced arbitrarily if a nongraphical method of determining the intensity curves were used, but the accuracy of the experimental data was not great enough to require greater theoretical accuracy here.

Also shown in Fig. 9 is α_m/α_0 versus ξ_0^2 derived from the third-order iterative solution, α_L of Eq. (76), for $\eta = 0.05$ and $\eta = 0.10$. The most important difference between the present and the iterative results is that α_m/α_0 tends to saturate with

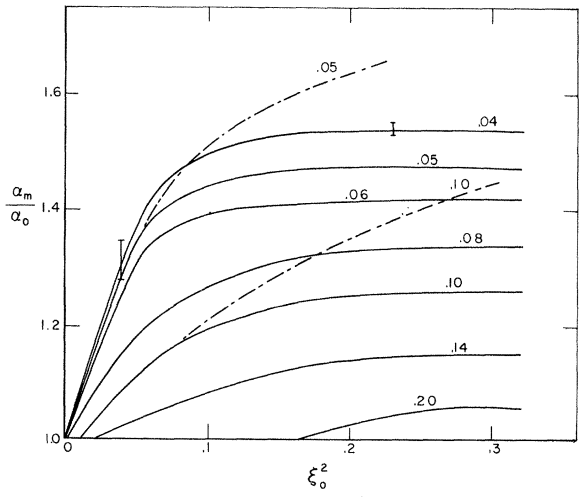

FIG. 9. α_m/α_0 as a function of ξ_0^2 and η, for a Maxwellian velocity distribution. The solid lines represent the present work; the dashed lines are from the third-order iterative solution, Eq. (76). The numbers on the curves denote values of $\eta \equiv \gamma_{ab}/Ku$.

increasing ξ_0^2 in the present work. We shall see later that this saturation is also a feature of the experimental curves, one which makes them impossible to fit with the iterative results except at very small ξ_0^2. It can also be seen that the value at which α_m/α_0 tends to saturate is a sensitive function of η and thus provides a good way of measuring η.

Figure 10(a) shows α_0 as a function of ξ_0^2 for $\eta = 0.05$ and for $\eta = 0.20$. The same plot for α_L is also shown; in this case, the curve of α_0 versus ξ_0^2 is independent of η. All the curves are linear up to about $\xi_0^2 = 0.1$. The departure from linearity exhibited by the present results, toward larger α_0, is the direction seen experimentally; the iterative solution departs from linearity in the wrong direction. The purpose of Fig. 10(b) will be discussed presently.

VI. EFFECT OF PHASE-CHANGING COLLISIONS

Several authors[7-9] have considered the effects of collisions on the intensity-versus-tuning curves of gas lasers, using intensity functions equivalent to α_L [Eq. (44)]. The purpose of this section is not to present a complete calculation of all the effects of collisions, but merely to show how phase-changing collisions can be taken into account when the present method of calculating the intensity is used. The final results should not be taken very seriously, since velocity-changing collisions are completely neglected.

Suppose that the collisions are such that ω_{ab} becomes $\omega_{ab}+g(t)$. Then Eq. (25) becomes

$$\dot{f}_{ab} - i[\nu - \omega_{ab} - g(t) + i\gamma_{ab}]f_{ab} = (\rho_{aa} - \rho_{bb})(e^{-iKz} - e^{iKz}) \,. \tag{45}$$

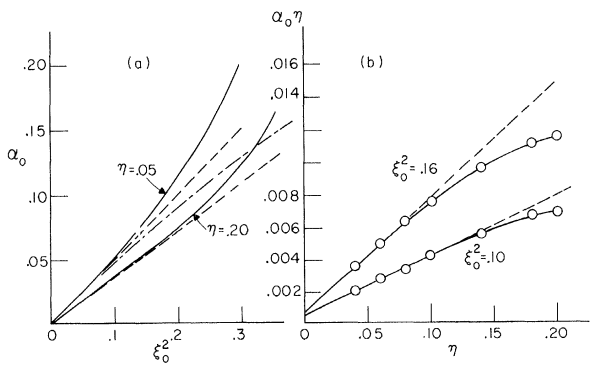

FIG. 10. (a) α_0, the intensity parameter at $(\nu - \omega_{ab}) = 0$, as a function of ξ_0^2 for a Maxwellian velocity distribution. The solid lines are from the present work; the dot-dashed lines are from the third-order iterative solution, Eq. (76). The dashed lines are straight lines drawn with the same initial slopes as α_0. (b) The quantity $\alpha_0\eta$ as a function of η from the present work, at two values of ξ_0^2. The dashed lines are straight lines with the same initial slopes as $\alpha_0\eta$.

Substituting

$$f_{ab} = \bar{f}_{ab}\, e^{i(\nu - \omega_{ab} + i\gamma_{ab})t}\, e^{-i\mu(t)} \,, \tag{46}$$

where $g(t) = \dfrac{d\mu(t)}{dt}$,

then, from Eq. (45),

$$\dot{\bar{f}}_{ab} = (\rho_{aa} - \rho_{bb}) e^{-i(\nu - \omega_{ab} + i\gamma_{ab})t} e^{i\mu(t)} (e^{-iKz} - e^{iKz}) \,,$$

and $\bar{f}_{ab} = \int_{-\infty}^{t} [\rho_{aa}(t') - \rho_{bb}(t')]$

$$\times [e^{-i(\nu - \omega_{ab} + i\gamma_{ab})t'} e^{i\mu(t')}][e^{-iKz(t')} - e^{iKz(t')}]\, dt' .$$

Using Eq. (46),

$$f_{ab} = \int_{-\infty}^{t} [\rho_{aa}(t') - \rho_{bb}(t')][e^{i(\nu - \omega_{ab} + i\gamma_{ab})(t-t')} e^{-i[\mu(t) - \mu(t')]}]$$

$$\times [e^{-iKz(t')} - e^{iKz(t')}] dt' . \tag{47}$$

Now suppose that $\mu(t) - \mu(t')$ depends only on $t - t' \equiv T$ and not on t or t', and replace $e^{-i[\mu(t) - \mu(t')]}$ by its average value over a time T. Also suppose, for now, that there is only one kind of collision, resulting in a phase change φ; this is generalized in Appendix E to include many different kinds of collisions. Then, if there are N collisions in time T, the phase change in time T is $N\varphi$. The probability of having N collisions in T is

$$(1/N!)(T/\tau_c)^N e^{-T/\tau_c} \,,$$

where τ_c is the average time between collisions. The average value of $e^{-i[\mu(t) - \mu(t')]}$ is then

$$\sum_{N=0}^{\infty} \frac{1}{N!} \left(\frac{T}{\tau_c}\right)^N e^{-T/\tau_c} e^{-iN\varphi} = e^{-T/\tau_c} \sum_{N=0}^{\infty} \frac{1}{N!} \left(\frac{T}{\tau_c} e^{-i\varphi}\right)^N$$

$$= e^{-T/\tau_c} e^{[(T/\tau_c)e^{-i\varphi}]} = e^{-\gamma_c T(1 - \cos\varphi + i\sin\varphi)} \,,$$

where $\gamma_c \equiv 1/\tau_c$. Equation (47) becomes

$$f_{ab} = \int_{-\infty}^{t} [\rho_{aa}(t') - \rho_{bb}(t')](e^{i(\nu - \omega_{ab} + i\gamma_{ab})(t-t')}$$

$$\times e^{-\gamma_c(1 - \cos\varphi + i\sin\varphi)(t-t')})(e^{-iKz(t')} - e^{iKz(t')}) dt'$$

$$= \int_{-\infty}^{t} [\rho_{aa}(t') - \rho_{bb}(t')][e^{i(\nu - \omega'_{ab} + i\gamma'_{ab})(t-t')}]$$

$$\times [e^{-iKz(t')} - e^{iKz(t')}] dt' ,$$

where $\omega'_{ab} \equiv \omega_{ab} + \gamma_c \sin\varphi$,

and $\gamma'_{ab} \equiv \gamma_{ab} + \gamma_c(1 - \cos\varphi)$.

Assume, as before, that

$$\rho_{aa}(t') - \rho_{bb}(t') = h_0 + \sum_{1}^{\infty} [h_n e^{2niKz(t')} + h_n^* e^{-2niKz(t')}] .$$

Then

$$f_{ab} = e^{i(\nu - \omega'_{ab} + i\gamma'_{ab})t} \int_{-\infty}^{t} e^{-i(\nu - \omega'_{ab} + i\gamma'_{ab})t'}$$

$$\times \left\{ \sum_{0}^{\infty} [(h_{n+1} - h_n)\, e^{(2n+1)iKz(t')} \right.$$

$$- (h_{n+1}^{*} - h_n^{*}) e^{-(2n+1)iKz(t')}\Big] \Big\} dt'$$

$$= -i \sum_0^{\infty} \left[\frac{b_n}{(\Delta_n^-)'} e^{(2n+1)iKz(t)} - \frac{b_n^*}{(\Delta_n^+)'} e^{-(2n+1)iKz(t)} \right],$$

where $(\Delta_n^-)' \equiv \nu - \omega'_{ab} - (2n+1)Kv_z + i\gamma'_{ab}$,

$(\Delta_n^+)' \equiv \nu - \omega'_{ab} + (2n+1)Kv_z + i\gamma'_{ab}$,

and $b_n = h_n - h_{n+1}$.

Substituting f_{ab} into Eqs. (23) and (24) as before, we find

$$h_0 = n_0 - 2\alpha \frac{\gamma_{ab}}{\gamma_{ab'}} \mathrm{Re}(b_0 R_0')$$

and $$h_n = -\alpha \frac{\gamma_{ab}}{\gamma'_{ab'}} (b_n R_n' - b_{n-1} R'_{n-1}) p_n, \quad n > 0$$

where $$R_n' \equiv i\gamma'_{ab} \left[\frac{1}{(\Delta_n^-)'} - \frac{1}{(\Delta_n^+)'^*} \right]$$

$$= i\gamma'_{ab} \left[\frac{1}{\nu - \omega'_{ab} - (2n+1)Kv_z + i\gamma'_{ab}} \right.$$

$$\left. - \frac{1}{\nu - \omega'_{ab} + (2n+1)Kv_z - i\gamma'_{ab}} \right].$$

Using $b_n \equiv n_0 B_n'$, the recursion relations are

$$B_0' = 1 - \alpha \frac{\gamma_{ab}}{\gamma'_{ab}} [2\mathrm{Re}(B_0' R_0') + (B_0' R_0' - B_1' R_1') p_1] ,$$

$$B_n' = \alpha \frac{\gamma_{ab}}{\gamma'_{ab}} [B'_{n+1} R'_{n+1} p_{n+1}$$

$$- B_n' R_n' (p_n + p_{n+1}) + B'_{n-1} R'_{n-1} p_n], \quad n > 0 .$$

Except for the p_n's, B_0' is the same function of

$$\omega'_{ab}, \ \gamma'_{ab}, \ \text{and} \ \alpha' \equiv \alpha(\gamma_{ab}/\gamma'_{ab}) ,$$

as B_0 was of α, ω_{ab}, and γ_{ab}. However, the presence of the p_n's, in which γ_a and γ_b are the zero-pressure values, changes the shape of the intensity curve from the zero-pressure shape. The p_n's become more important at higher intensities, however, so that for $\mathfrak{N}^{-1}$ greater than about 0.85 and for low pressures, one can expect the shape of the intensity curves to be approximately the same as the zero-pressure shapes, with $\alpha \to \alpha'$, $\omega_{ab} \to \omega'_{ab}$, and $\gamma_{ab} \to \gamma'_{ab}$. Since τ_c, the mean time between collisions, is proportional to the reciprocal of the density of atoms, one expects γ'_{ab} and ω'_{ab} to be linear functions of the density, at least at moderately low pressures.

Figure 10(b) shows that the quantity $\alpha_0\eta$ is a linear function of η for η smaller than about 0.1. (For the iterative solution, α_0 is independent of η, so that $\alpha_0\eta$ is automatically proportional to η.) In the case of pressure broadening, $\alpha_0 \to \alpha_0'$, so that $\alpha_0'\eta'$ should be a linear function of η'. Since the absolute height at the center of a pressure-broadened intensity curve is proportional to $\alpha_0 = \alpha_0'\gamma'_{ab}/\gamma_{ab} = \alpha_0'\eta'/\eta$, the height should also be proportional to η', for η' less than 0.1.

Of course, these conclusions are valid only for the case of pure Lorentz broadening, or if the velocity-changing collisions affect the intensity curves in the same way as do the phase-changing collisions. Nevertheless, in Sec. VII experimental curves taken at different pressures are analyzed under the assumption that only ω_{ab}, γ_{ab}, and the magnitudes of the curves change with pressure, not the shapes. The fact that this turns out to be a good assumption indicates that either velocity-changing collisions are not important at these pressures or that they have the same effect on the intensity as the phase-changing collisions.

VII. EXPERIMENTAL RESULTS

Figure 11 shows typical curves of intensity (I) versus cavity tuning (x) obtained using a 31-cm-long hemispherical He^3-Ne^{20} laser, operating at a wavelength of 1.15 μm and a pressure of 0.2 Torr pure neon. The different curves correspond to different levels of excitation, i.e., to different values of the relative inversion density $\mathfrak{N}$. Both I and x are in arbitrary units. The cavity length was was changed by means of a piezoelectric crystal (PZT) on which the flat mirror was mounted. In general, this method of changing the length introduces several kinds of distortion into the intensity curves. These are discussed in Appendix F. The curves of Fig. 11 have not been corrected for PZT

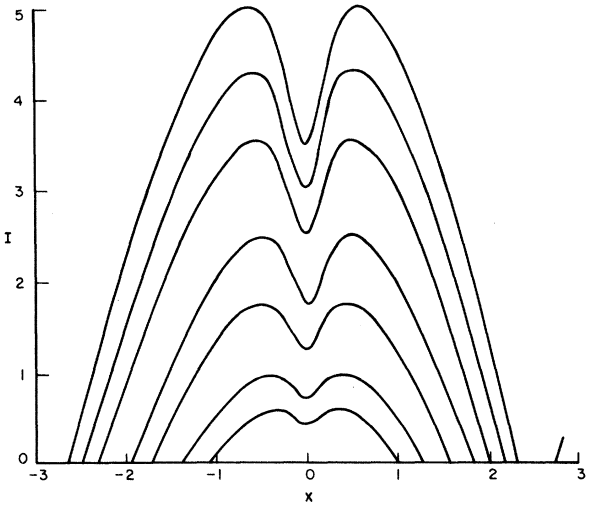

FIG. 11. Experimental intensity-versus-tuning curves taken at a pressure of 0.2 Torr pure neon. I is the intensity and x the nominal cavity length, both in arbitrary units. The different curves correspond to different discharge currents, and thus to different values of the inversion density $\mathfrak{N}$.

distortion except that their centers have been shifted slightly to coincide with one another. They are typical of all the data used here in that there is no detectable difference in the heights of the two maxima, but the abscissa is distorted by the nonlinear dependence of the *PZT* length on applied voltage.

The order separation is $c/2L = 485$ MHz. The temperature was obtained by measuring the Doppler width of spontaneously emitted 6328-Å light with a Fabry-Perot interferometer; $Ku/2\pi$ for the 1.15-μm line was 580 ± 30 MHz, corresponding to a temperature of about 250 °C. (In this and in subsequent cases, stated uncertainties represent an estimated 90% confidence level.) The temperature actually changes slightly with pressure and with discharge current, but sufficient accuracy was obtained by using an average temperature. For each intensity curve, three quantities were measured: I_m, the intensity at the maximum; I_0, the intensity at the center (both in arbitrary units); and $2x_0$, the width of the curve at the bottom. $2x_0$, Ku, and the known order separation determine ξ_0.

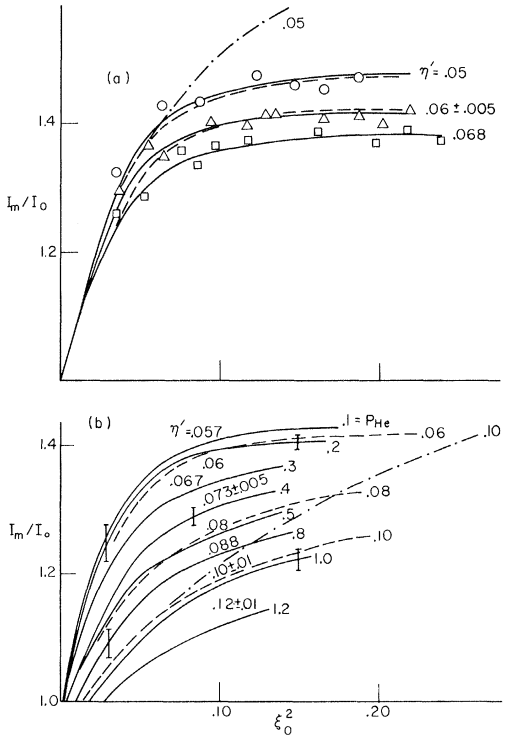

FIG. 12. (a) Points are experimental values of I_m/I_0 as a function of ξ_0^2, for three different pressures of pure neon: 0.1 Torr (circles), 0.2 Torr (triangles), and 0.3 Torr (squares). The solid lines were drawn through the experimental points. The dashed lines are α_m/α_0 as a function of ξ_0^2 from the present work, for $\eta = 0.05$ and 0.06. The dot-dashed line is α_m/α_0 from the third-order iterative solution, for $\eta = 0.05$. The other numbers indicate the experimental values of η' deduced by matching and theoretical (dashed) curves to the experimental ones. (b) These curves represent the same quantities as those of (a), for He-Ne mixtures. Here, the neon pressure is fixed at 0.1 Torr, and the helium pressure varies from 0.1 to 1.2 Torr. The error bars indicate experimental errors. The numbers on the experimental curves are the experimental values of η'. The helium pressure in Torr are at the ends of the experimental curves. The theoretical values of η are at the ends of the theoretical curves.

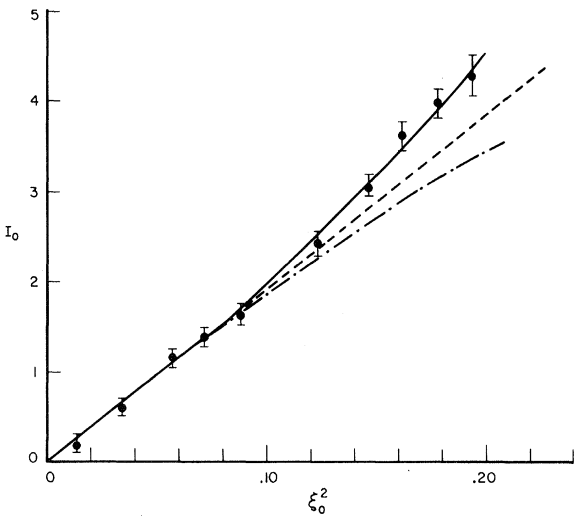

FIG. 13. Points are experimental values of I_0 as a function of ξ_0^2, in arbitrary units. The solid line is α_0 versus ξ_0^2 from the present work, and the dot-dashed curve is α_0 versus ξ_0^2 from the third-order iterative solution. The theoretical curves have been normalized to have the same initial slope as the experimental points.

The agreement between the present theory and experiment is shown in Fig. 12, where experimental values of I_m/I_0 are plotted against ξ_0^2, for several different pressures. (Each curve in Fig. 12 corresponds to a set of intensity curves such as those shown in Fig. 11.) Theoretical plots of α_m/α_0 taken from Fig. 9, for several values of η, are also shown. The shapes of the curves of Figs. 9 and 12 agree quite well, to within the errors; this constitutes a good test of the theory. Also shown in Fig. 12 is the third-order iterative result. It can be seen that, although a fit can be made to experiment at any particular value of ξ_0^2 (or for all ξ_0^2 from 0 to about 0.075), there is no way of adjusting η to make the entire curve fit an experimental one. Figure 12(a) is for pure neon in the pressure range 0.1–0.3 Torr (the only pressure at which laser action could be obtained in pure neon). In Fig. 12(b), the neon pressure is held fixed at 0.1 Torr, and the helium pressure is changed from 0.1 to 1.2 Torr. Also shown are the values of η' deduced by comparison with curves such as those in Fig. 9.

Figure 13 shows I_0 versus ξ_0^2 for the case of

0.1-Torr pure neon. The solid line is the predicted behavior, taken from Fig. 10(a) for $\eta = 0.05$. The theoretical and experimental results were normalized to the same initial slopes, so that the only reason for showing this curve is to show that the theoretical departure from linearity is in the same direction as the experimental. Also shown is the third-order result, which deviates from linearity in the wrong direction above $\xi_0^2 \cong 0.1$.

In Figs. 14(a) and 14(b), the values of η' from Fig. 12 are plotted against pressure; to within the errors, η' goes up linearly with pressure, although the errors are rather large, especially in the pure-neon case where there are not many points. The extrapolated zero-pressure value of η' in Fig. 14(a) is $\eta_0 = 0.04 \pm 0.01$. η_0 might be considered to be $\eta \equiv \gamma_{ab}/Ku$, but there is some question about whether or not η' is linear with pressure at very low pressures. Also, it is not well established by the data that η' is really a linear function of pressure at the higher pressures, and it is not clear that it should be, since the theory is so approximate. In any case, if $\eta_0 Ku \equiv (\gamma_{ab})_0$, then

$$\frac{(\gamma_{ab})_0}{2\pi} = \frac{(\gamma_a + \gamma_b)_0}{4\pi} = 23 \pm 7 \text{ MHz}.$$

The magnitude of the collisional line broadening implied by Figs. 14(a) and 14(b) is equivalent to a change in $\gamma'_{ab}/2\pi$ of 61 ± 14 MHz per room-temperature Torr of helium and of 107 ± 35 MHz per room-temperature Torr of neon.

Szöke and Javan[8] have also measured the effects of collisions on the 1.15-μ laser intensity, but it is not possible to compare our results directly with theirs, because their theory is designed to account for deviations from the third-order iterative solution present in their tuning curves through the use of two different γ'_{ab}'s, and a quantity $\Delta^{(1)}$. That is, instead of Eq. (44) they use

$$\alpha = K\left\{G_0 - L\exp\left[\left(\frac{\nu - \omega_{ab} - \Delta^{(1)}}{Ku}\right)^2\right]\left(1 + \frac{\gamma\gamma'}{(\nu - \omega_{ab})^2 + (\gamma')^2}\right)^{-1}\right\},$$

where $\gamma' > \gamma$. Also, they were not able to measure their temperature and therefore used the room-temperature value of $Ku/2\pi$, 450 MHz, which introduces a large uncertainty into the conversion of η' to γ'_{ab}. Both the "hard" and "soft" line half-widths used in their analysis extrapolate to about 11 MHz at zero pressure; this is different from our $(\gamma_{ab})_0$ by about a factor 2.0 ± 0.5. However, there are many factors in both experiments which could account for such a disagreement, as discussed above.

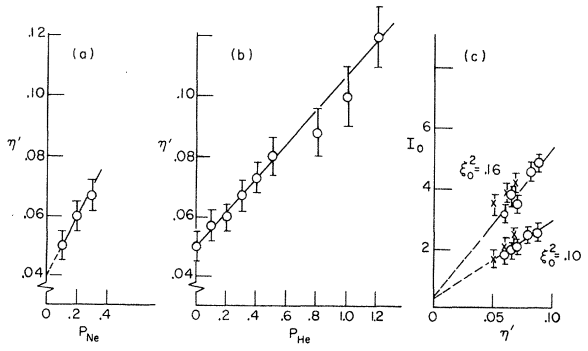

FIG. 14. (a) Experimental values of η' as a function of neon pressure for pure neon. (b) The experimental values of η' as a function of helium pressure for a fixed neon pressure of 0.1 Torr. (c) I_0 in arbitrary units versus η', for two values of ξ_0^2. The crosses are for the pure neon case, the circles for the He-Ne mixtures.

Figure 14(c) shows I_0, the height at the center of the intensity curve, for specified values of ξ_0^2, plotted against the η''s obtained from Fig. 12. For pure Lorentz broadening, I_0 should be proportional to η', as discussed in Sec. VI. There might be a small difference between the pure neon data and the neon-helium data, but the errors are too large to be able to tell. In any case, I_0 does seem to be more or less proportional to η'. If it were true that no difference exists between the pure neon and the neon-helium cases in Fig. 14(c), this would be good evidence for the validity of the intensity curve shapes given in Sec. VI; it would show the shape to be independent of the specific broadening mechanism, which must be quite different in the two cases, and only dependent on some net η'.

Thus, there seems to be good agreement between theory and experiment, at least up to $\alpha \cong 0.2$. It would be useful, however, to test the present theory with a shorter laser, in which even higher single-mode intensities could be obtained. On the other hand, the pressure would probably have to be higher to obtain enough gain in a shorter laser, so that unknown pressure effects might become more important.

VIII. SUMMARY OF RESULTS

We have shown that the use of rate terms to account for the production of atoms in the two levels gives results equivalent to those obtained by Lamb[1] and simplifies the calculation enough to allow the iterative solution to be extended to higher order. With the higher-order terms, the iterative solution could be seen to be asymptotic and it was shown to be useful only for α of the order of $0 \rightarrow 0.05$. Then a noniterative solution was obtained, in the form of a Fourier series, with coefficients determined by recursion relations. A method of solving the recursion equations was

developed, and calculated laser intensities for both flat and Maxwellian velocity distributions were presented. A method of calculating the effects of phase-changing collisions was developed. Experimental data for a 1.15-μm laser were compared to the theory and showed good agreement, to within the errors.

ACKNOWLEDGMENTS

I am grateful to Dr. Peter Bender and Dr. Frank Olver for many useful discussions.

APPENDIX A: ITERATIVE SOLUTION

For $\alpha = 0$ the solution to the recursion relations is

$$B_0^{(0)} = 1, \quad B_n^{(0)} = 0, \quad n \neq 0 .$$

This is equivalent to the first-order solution in Ref. 1. (There is another factor of E in ρ_{ab} so that this solution is first order in the electric field.) The third-order solution is

$$B_0^{(1)} = 1 - \alpha\,[2\,\mathrm{Re}(B_0^{(0)}R_0) + (B_0^{(0)}R_0 - B_1^{(0)}R_1)p_1]$$
$$= 1 - \alpha\,[2\,\mathrm{Re}R_0 + R_0 p_1] = 1 - \alpha\,[R_0 + R_0^* + R_0 p_1] ,$$
$$B_1^{(1)} = \alpha\,[B_2^{(0)}R_2^{(0)}p_2 - B_1^{(0)}R_1^{(0)}(p_1+p_2) + B_0^{(0)}R_0 p_1]$$
$$= \alpha R_0 p_1 ,$$
$$B_2^{(1)} = B_3^{(1)} = \cdots = 0 .$$

The fifth-order solution for B_0 is

$$B_0^{(2)} = 1 - \alpha\,(R_0 + R_0^* + R_0 p_1) + \alpha^2\,[R_0(R_0 + R_0^* + R_0 p_1)$$
$$+ R_0^*(R_0^* + R_0 + R_0^* p_1^*)$$
$$+ R_0 p_1 (R_0 + R_0^* + R_0 p_1 + R_1 p_1)] .$$

For a Maxwellian velocity distribution,

$$J = \frac{1}{\sqrt{\pi}} \int_{-\infty}^{\infty} \mathrm{Re}(B_0 R_0)\, e^{-(v_z/u)^2} \frac{dv_z}{u} .$$

In the Doppler limit ($\gamma_{ab}/Ku \to 0$), and for small α,

$$e^{-(v_z/u)^2} \cong e^{-[(\nu-\omega_{ab})/Ku]^2}$$

because of the factor R_0 and

$$J \cong \frac{e^{-[(\nu-\omega_{ab})/Ku]^2}}{\sqrt{\pi}u} \int_{-\infty}^{\infty} \mathrm{Re}(B_0 R_0)\, dv_z$$
$$= \frac{e^{-[(\nu-\omega_{ab})/Ku]^2}}{\sqrt{(\pi)}u}\, \mathrm{Re} \int_{-\infty}^{\infty} B_0 R_0\, dv_z .$$

Using contour integration, one finds

$$J = 2\sqrt{\pi}\,\frac{\gamma_{ab}}{Ku} \exp\left[-\left(\frac{\nu-\omega_{ab}}{Ku}\right)^2\right]$$
$$\times \mathrm{Re}[1 - \alpha F_0 + \tfrac{1}{2}\alpha^2 F_0^2 (3 + 2G_1) \cdots] ,$$

where $$F_0 \equiv 1 + \frac{i\gamma_{ab}}{\nu - \omega_{ab} + i\gamma_{ab}} ,$$

and $$G_1 \equiv \frac{i\gamma_a\gamma_b}{4\gamma_{ab}} \left[\frac{1}{\nu - \omega_{ab} - i\,(\gamma_{ab} + \frac{1}{2}\gamma_a)} + \frac{1}{\nu - \omega_{ab} - i\,(\gamma_{ab} + \frac{1}{2}\gamma_b)}\right] .$$

Since $J_T = 2\sqrt{(\pi)}\,(\gamma_{ab}/Ku)$,

the equation determining α is

$$\frac{J}{J_T} = \exp\left[-\left(\frac{\nu-\omega_{ab}}{Ku}\right)^2\right]$$
$$\times \mathrm{Re}[1 - \alpha F_0 + \tfrac{1}{2}\alpha^2 F_0^2 (3 + 2G_1) - \cdots] = \mathfrak{N}^{-1} .$$

Through third order,

$$\exp\left[-\left(\frac{\nu-\omega_{ab}}{Ku}\right)^2\right] \mathrm{Re}[1 - \alpha F_0] = \mathfrak{N}^{-1}$$

or $$\alpha = 1 - \mathfrak{N}^{-1} \exp\left[\left(\frac{\nu-\omega_{ab}}{Ku}\right)^2\right] \left(1 + \frac{\gamma_{ab}^2}{(\nu-\omega_{ab})^2 + \gamma_{ab}^2}\right)^{-1} .$$

This is the same as the results of Refs. 1 and 2 except for the fact that they have

$$\exp\left[-\left(\frac{\nu-\omega_{ab}}{Ku}\right)^2\right] - \mathfrak{N}^{-1}$$

in the numerator, which is not important because $(\nu - \omega_{ab})/Ku$ is supposed to be small.

If $\gamma_a = \gamma_b$ and $\nu = \omega_{ab}$, then $F_0 = 2$ and $G_1 = \frac{1}{3}$ so that

$$J/J_T = 1 - 2\alpha + 2\alpha^2 (3 + \tfrac{2}{3}) - \cdots .$$

The series for J/J_T seems to be asymptotic. That

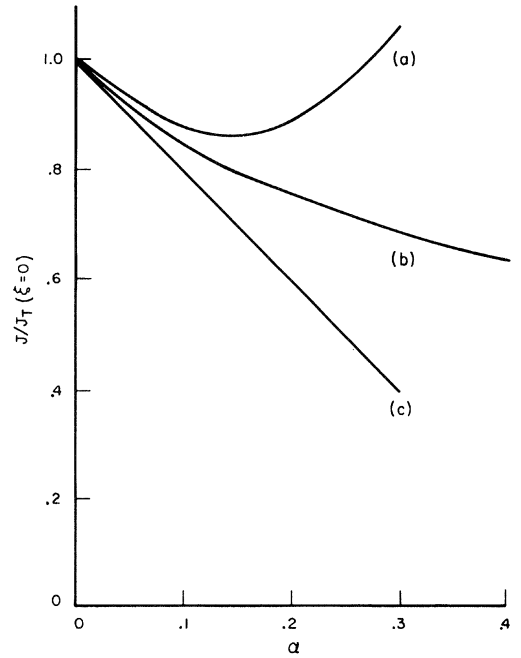

FIG. 15. J/J_T as a function of α at $\xi = 0$ ($\nu - \omega_{ab} = 0$). (a) is the fifth-order iterative solution; (b) is the present work; and (c) is the third-order iterative result.

is, it is divergent but, if α is very small, the series can still represent J/J_T fairly well. J/J_T obtained here is compared to the solution obtained in the present work in Fig. 15. Deviations of the order of 10% in J/J_T occur above $\alpha \cong 0.1$ in both the third- and fifth-order solutions. Figure 15 also shows that α is in error by more than 20% for α greater than about 0.05, because of the way α depends on J/J_T.

In the series for J/J_T, the third term (the α^2 term) equals the second one (the α term) at $\alpha = 0.3$, and subsequent terms are even larger, so that no improvement results from including more terms. The convergence is somewhat better for large $(\nu - \omega_{ab})/Ku$, where F_0 and G_1 are smaller.

APPENDIX B: CONVERGENCE OF SERIES FOR ρ_{ab}

$$\rho_{ab} = -i\left(\frac{\wp E}{4\hbar}\right) n_0 e^{-i(\nu t+\rho)} \times \sum_0^\infty \left(\frac{B_n}{\Delta_n^-} e^{(2n+1)iKz} - \frac{B_n^*}{\Delta_n^+} e^{-(2n+1)iKz} \right).$$

ρ_{ab} converges if

$$\lim_{n\to\infty} \left| \frac{(B_n/\Delta_n^-) e^{(2n+1)iKz}}{(B_{n-1}/\Delta_{n-1}^-) e^{(2n-1)iKz}} \right| < 1 ,$$

with a similar requirement for B_n^*/Δ_n^+, or if

$$\lim_{n\to\infty} \left| \frac{B_n[\nu - \omega_{ab} - (2n-1)Kv_z + i\gamma_{ab}]}{B_{n-1}[\nu - \omega_{ab} - (2n+1)Kv_z + i\gamma_{ab}]} \right| = \lim_{n\to\infty} \left| \frac{B_n}{B_{n-1}} \right| < 1 .$$

For large n, the recursion relations give

$$\alpha B_{n+1} R_{n+1} p_{n+1} - B_n[1 + \alpha R_n(p_n + p_{n+1})] + \alpha B_{n-1} R_{n-1} p_n = 0 .$$

Dividing by B_{n-1},

$$\alpha \frac{B_{n+1}}{B_n} \frac{B_n}{B_{n-1}} R_{n+1} p_{n+1} - \frac{B_n}{B_{n-1}}[1 + \alpha R_n(p_n + p_{n+1})] + \alpha R_{n-1} p_n = 0 .$$

Except for the case $v_z = 0$, which is considered elsewhere, $R_n \to 0$ and $p_n \to 0$ as $n \to \infty$. Thus,

$$\lim_{n\to\infty} \frac{B_n}{B_{n-1}} \left[\alpha \frac{B_{n+1}}{B_n} R_{n+1} p_{n+1} - 1 \right] = 0$$

and either (a) $$\lim_{n\to\infty} \frac{B_n}{B_{n-1}} = 0$$

or (b) $$\lim_{n\to\infty} \left[\alpha \frac{B_{n+1}}{B_n} R_{n+1} p_{n+1} - 1 \right] = 0 .$$

Case (b) is $$\lim_{n\to\infty} \frac{B_n}{B_{n-1}} = \frac{1}{\alpha R_n p_n} \to \infty ,$$

and is thus the divergent solution. Case (a) is the desired convergent solution.

APPENDIX C: SOLUTION TO RECURSION EQUATIONS FOR CASE $v_z = 0$

If $v_z = 0$,

$$R_0 = R_1 = R_2 = \cdots = \frac{2\gamma_{ab}^2}{(\nu - \omega_{ab})^2 + \gamma_{ab}^2} \equiv R ,$$

and $$p_1 = p_2 = \cdots = 1 ,$$

then
$$B_0 = 1 - \alpha R(3B_0 - B_1) ,$$
$$B_1 = \alpha R(B_2 - 2B_1 + B_0) ,$$
$$\vdots$$

or
$$\alpha R B_1 - (1 + 3\alpha R) B_0 + 1 = 0 , \quad \text{(C1)}$$
$$\alpha R B_2 - (1 + 2\alpha R) B_1 + \alpha R B_0 = 0 , \quad \text{(C2)}$$
$$\vdots$$
$$\alpha R B_{n+1} - (1 + 2\alpha R) B_n + \alpha R B_{n-1} = 0 , \quad \text{(C3)}$$
$$\vdots$$

The solution to these equations is

$$B_n = a\lambda_1^n + b\lambda_2^n ,$$

where λ_1 and λ_2 are solutions to

$$\alpha R \lambda^2 - (1 + 2\alpha R)\lambda + \alpha R = 0 ,$$

and a and b are constants to be determined later. Thus,

$$\lambda_1 = 1 + \frac{1}{2\alpha R} + \left[\left(1 + \frac{1}{2\alpha R} \right)^2 - 1 \right]^{1/2} > 1 ,$$

$$\lambda_2 = 1 + \frac{1}{2\alpha R} - \left[\left(1 + \frac{1}{2\alpha R} \right)^2 - 1 \right]^{1/2} < 1 .$$

Since λ_1 is greater than 1, we must have $a = 0$ for a convergent solution. Then

$$B_n / B_{n-1} = \lambda_2 < 1$$

as desired. The other constant b, is fixed by Eq. (C1):

$$\alpha R b \lambda_2 - (1 + 3\alpha R) b + 1 = 0 ,$$

$$b = \frac{2}{1 + 4\alpha R + (1 + 4\alpha R)^{1/2}} = B_0 .$$

The following will show that this solution is the same as the exact one:

$$f_{ab} = -in_0 \sum_0^\infty \left(\frac{B_n}{\Delta_n^-} e^{(2n+1)iKz} - \frac{B_n^*}{\Delta_n^+} e^{-(2n+1)iKz} \right) .$$

For $v_z = 0$, we have

$$f_{ab} = \frac{2n_0}{(\nu - \omega_{ab} + i\gamma_{ab})} \sum_0^\infty B_n \sin[(2n+1)Kz] = \left(\frac{2n_0}{\nu - \omega_{ab} + i\gamma_{ab}} \right) \left(\frac{2}{1 + 4\alpha R + (1 + 4\alpha R)^{1/2}} \right)$$

$$\times\sum_0^\infty \lambda_2^n \sin[(2n+1)Kz] \ ,$$

$$\sum_0^\infty \lambda_2^n \sin[(2n+1)Kz] = \frac{1}{2i}\sum_0^\infty \lambda_2^n [\, e^{(2n+1)iKz} - e^{-(2n+1)iKz}]$$

$$= \frac{1}{2i}\left[\frac{e^{iKz}}{1-\lambda_2 e^{2iKz}} - \frac{e^{-iKz}}{1-\lambda_2 e^{-2iKz}}\right]$$

$$= \frac{\sin Kz(1+\lambda_2)}{(1-\lambda_2)^2 + 4\lambda_2 \sin^2 Kz} \ .$$

Then, we have

$$f_{ab} = \left(\frac{4n_0}{\nu - \omega_{ab} + i\gamma_{ab}}\right)\left(\frac{1}{1+4\alpha R+(1+4\alpha R)^{1/2}}\right) \times\left(\frac{\sin Kz(1+\lambda_2)}{(1-\lambda_2)^2+4\lambda_2\sin^2 Kz}\right)$$

$$= \frac{2n_0 \sin Kz}{(\nu-\omega_{ab}+i\gamma_{ab})(1+4\alpha R\sin^2 Kz)}$$

$$= \frac{2n_0 \sin Kz(\nu-\omega_{ab}-i\gamma_{ab})}{(\nu-\omega_{ab})^2+\gamma_{ab}^2(1+8\alpha\sin^2 Kz)} \ .$$

This solution is also obtainable from Eqs. (23) – (25) (see also Ref. 1). If $v_z = 0$, then $z = \bar{z}$, a constant, and one can set $\dot{\rho}_{aa} = \dot{\rho}_{bb} = \dot{f}_{ab} = 0$ in Eqs. (23) – (25). The above result is then easily obtained.

APPENDIX D: EXPLICIT EXPRESSIONS FOR $G(v_z)$

In case A, $B_1 = B_2 = \cdots = 0$. From Eq. (54), B_0 is the solution to

$$B_0 = 1 - \alpha[2\,\mathrm{Re}(B_0 R_0) + B_0 R_0 p_1] \ ,$$

which is

$$B_0^{(A)} = \frac{Q_0^{(0)*} - \alpha R_0^*}{Q_0^{(0)} Q_0^{(0)*} - \alpha^2 R_0 R_0^*} \ .$$

Here, we have $Q_0^{(0)} \equiv 1 + \alpha R_0(1+p_1)$.

Then we obtain

$$G^{(A)}(v_z) = \mathrm{Re}(B_0^{(A)} R_0) = \frac{\mathrm{Re}[(Q_0^{(0)*} - \alpha R_0^*)R_0]}{Q_0^{(0)} Q_0^{(0)*} - \alpha^2 R_0 R_0^*} \ .$$

In case B, $B_2 = B_3 = \cdots = 0$, and B_1 is the solution to [Eq. (55)]

$$B_1 = \alpha[-B_1 R_1(p_1+p_2) + B_0 R_0 p_1]$$

or $$B_1 = \left(\frac{\alpha R_0 p_1}{Q_1^{(0)}}\right) B_0 \ ,$$

where $$Q_1^{(0)} \equiv 1 + \alpha R_1(p_1+p_2) \ .$$

Then B_0 is the solution to

$$B_0 = 1 - \alpha\left[2\,\mathrm{Re}(B_0 R_0) + B_0 R_0 p_1 - \frac{\alpha R_0 R_1 p_1^2}{Q_1^{(0)}} B_0\right] ,$$

which is $$B_0^{(B)} = \frac{Q_0^{(1)*} - \alpha R_0^*}{Q_0^{(1)} Q_0^{(1)*} - \alpha^2 R_0 R_0^*} \ ,$$

where $$Q_0^{(1)} = Q_0^{(0)} - \frac{\alpha^2 R_0 R_1 p_1^2}{Q_1^{(0)}} \ .$$

Similar methods yield, for case C, $B_3 = B_4 = \cdots = 0$,

$$B_0^{(c)} = \frac{Q_0^{(2)*} - \alpha R_0^*}{Q_0^{(2)} Q_0^{(2)*} - \alpha^2 R_0 R_0^*} \ ,$$

where $$Q_0^{(2)} = Q_0^{(0)} - \frac{\alpha^2 R_0 R_1 p_1^2}{Q_1^{(0)} - \alpha^2 R_1 R_2 p_2^2 / Q_2^{(0)}} \ .$$

Here we have

$$Q_2^{(0)} = 1 + \alpha R_2(p_2+p_3) \ .$$

It can be seen that the $Q_0^{(n)}$'s and hence the different cases, differ most for large α and for large $R_0 R_1 p_1^2$ ($\nu = \omega_{ab}$ and $v_z = 0$). Also, if p_1 is small (v_z large), then we have

$$Q_0^{(0)} \cong 1 + \alpha R_0 \quad \text{and} \quad B_0 \cong [1 + \alpha(R_0 + R_0^*)]^{-1} \ .$$

APPENDIX E: EFFECT OF SEVERAL KINDS OF PHASE-CHANGING COLLISIONS

Suppose that there are three kinds of collisions 1, 2, and 3, with cross sections σ_1, σ_2, and σ_3, respectively. The total collision cross section σ_c is

$$\sigma_c = \sigma_1 + \sigma_2 + \sigma_3 \ . \tag{E1}$$

The mean time between collisions of type 1, τ_1, is proportional to $1/\sigma_1$, etc. The probability of n_1 collisions of type 1, n_2 of type 2, etc., in time T is

$$\frac{1}{n_1!}\left(\frac{T}{\tau_1}\right)^{n_1} e^{-T/\tau_1} \frac{1}{n_2!}\left(\frac{T}{\tau_2}\right)^{n_2} e^{-T/\tau_2} \frac{1}{n_3!}\left(\frac{T}{\tau_3}\right)^{n_3} e^{-T/\tau_3} \tag{E2}$$

From Eq. (E1), we have

$$\frac{1}{\tau_1} + \frac{1}{\tau_2} + \frac{1}{\tau_3} = \frac{1}{\tau_c}$$

and $$\frac{1}{\tau_1} = \frac{\sigma_1}{\sigma_c}\frac{1}{\tau_c} \ , \quad \frac{1}{\tau_2} = \frac{\sigma_2}{\sigma_c}\frac{1}{\tau_c} \ , \text{ etc.}$$

Equation (E2) becomes

$$\frac{1}{n_1! n_2! n_3!}\left(\frac{\sigma_1}{\sigma_c}\right)^{n_1}\left(\frac{\sigma_2}{\sigma_c}\right)^{n_2}\left(\frac{\sigma_3}{\sigma_c}\right)^{n_3}\left(\frac{T}{\tau_c}\right)^{n_1+n_2+n_3} e^{-T/\tau_c} \ .$$

Suppose that a collision of type 1 causes a phase change of φ_1, etc. Then, if there are n_1 collisions of type 1, etc.,

$$e^{-i[\mu(t)-\mu(t')]} \to e^{-i[n_1\varphi_1+n_2\varphi_2+n_3\varphi_3]}$$

and the average value of $e^{-i[\mu(t)-\mu(t')]}$ over time $T=t-t'$ is

$$\sum_{n_1=0}^{\infty}\sum_{n_2=0}^{\infty}\sum_{n_3=0}^{\infty}\frac{1}{n_1!\,n_2!\,n_3!}\left(\frac{\sigma_1}{\sigma_c}\right)^{n_1}$$

$$\times\left(\frac{\sigma_2}{\sigma_c}\right)^{n_2}\left(\frac{\sigma_3}{\sigma_c}\right)^{n_3}\left(\frac{T}{\tau_c}\right)^{n_1+n_2+n_3}$$

$$\times e^{-T/\tau_c}e^{-i[n_1\varphi_1+n_2\varphi_2+n_3\varphi_3]}$$

$$=e^{-T/\tau c}e^{[(\sigma_1/\sigma c)(T/\tau c)e^{-i\varphi_1}]}e^{[(\sigma_2/\sigma c)(T/\tau c)e^{-i\varphi_2}]}$$

$$\times e^{[(\sigma_3/\sigma c)(T/\tau c)e^{-i\varphi_3}]}$$

$$=e^{-T/\tau c[1-(\sigma_1/\sigma c)\cos\varphi_1-(\sigma_2/\sigma c)\cos\varphi_2\cdots+i(\sigma_1/\sigma c)\sin\varphi_1\cdots}$$

$$=e^{-T/\tau c[(1-\cos\varphi)_{av}+i(\sin\varphi)_{av}]},$$

where $(1-\cos\varphi)_{av}=\sum_{i=1}^{3}\frac{\sigma_i}{\sigma_c}(1-\cos\varphi_i)$,

$$(\sin\varphi)_{av}=\sum_{i=1}^{3}\frac{\sigma_i}{\sigma_c}\sin\varphi_i,$$

or, in the case of N collisions,

$$(1-\cos\varphi)_{av}=\sum_{i=1}^{N}\frac{\sigma_i}{\sigma_c}(1-\cos\varphi_i),$$

$$(\sin\varphi)_{av}=\sum_{i=1}^{N}\frac{\sigma_i}{\sigma_c}\sin\varphi_i.$$

Thus, $\omega'_{ab}=\omega_{ab}+\gamma_c(\sin\varphi)_{av}$

and $\gamma'_{ab}=\gamma_{ab}+\gamma_c(1-\cos\varphi)_{av}$.

APPENDIX F: *PZT* DISTORTION OF INTENSITY CURVES

One kind of distortion is due to tilt of the *PZT* as it changes length; depending on the mirror alignment and on the mode geometry, the tilt can introduce loss changes as the intensity curve is swept, so that the two maxima appear to have different heights. Such an asymmetry can sometimes be distinguished from any true asymmetry in the curve by its tendency to change with time, with mirror alignment, and from one order to another (although the latter effect could be due to something else, such as gain at 3.39 μm). Since the laser intensity is a complicated function of the cavity loss, there does not seem to be a reliable way of correcting for tilt. Fortunately, there was no detectable difference in the two maxima of the intensity curves obtained here over the pressure range used, although such differences have been seen at other times with different mirror alignment.

Another kind of distortion is caused by the fact that the length of the *PZT* is a nonlinear function of the applied voltage; this distorts the horizontal axis of the intensity curves, and can be detected by measuring the change in order separation with *PZT* voltage. This effect was about 10% per order in the present work and was corrected for approximately, although the results are not sensitive to this kind of distortion. Another distortion is due to hysteresis in the *PZT*; if one sweeps through the same curve twice in succession, the centers of the two curves will be displaced from each other. Many of these problems can be avoided, either by using better crystals or by using a pressure scan (which, however, may also introduce loss changes). Since the distortions did not affect the present work substantially, no attempt was made to improve the sweep. It is evident, however, that there is some difficulty in distinguishing true asymmetries in the intensity curves from instrumental ones. For these reasons, any small asymmetries in the heights of the two maxima were assumed to be undetectable, and all asymmetries in the horizontal axis were attributed to instrumental effects.

---

[1]W. E. Lamb, Jr., Phys. Rev. 134, A1429 (1964).

[2]W. R. Bennett, Jr., Phys. Rev. 126, 580 (1962); in *Proceeding of the Third International Conference on Quantum Electronics, Paris*, 1963 edited by P. Grivet and N. Bloembergen, (Columbia U. P., New York, 1964).

[3]K. Uehara and K. Shimoda, Japan. J. Appl. Phys. 4, 921 (1965).

[4]Howard Greenstein, Phys. Rev. 175, 438 (1968).

[5]N. L. Balazs and I. Tobias, Phil. Trans. Roy. Soc. London 264, 1 (1969).

[6]S. Stenholm and W. E. Lamb, Jr., Phys. Rev. 181, 618 (1969).

[7]R. L. Fork and M. A. Pollack, Phys. Rev. 139, A1408 (1965).

[8]A. Szöke and A. Javan, Phys. Rev. 145, 137 (1966).

[9]B. L. Gyorffy, M. Borenstein, and W. E. Lamb, Jr., Phys. Rev. 169, 340 (1968).